RSC Advances

PAPER

View Article Online
View Journal | View Issue

Cite this: *RSC Adv.*, 2018, **8**, 38047

Preparation of a superfine RDX/Al composite as an energetic material by mechanical ball-milling method and the study of its thermal properties

Lei Xiao,[a] Yan Zhang,[b] Xiaohong Wang,*[b] Gazi Hao,[a] Jie Liu,[a] Xiang Ke,[a] Teng Chen[a] and Wei Jiang*[a]

To research the influence of aluminum (Al) on the decomposition of 1,3,5-trimethylene trinitramine (RDX), a type of superfine RDX/Al composite as an energetic material with a mass ratio of 70/30 was successfully prepared by mechanical ball-milling method. The morphology and structure of the superfine RDX/Al composite were characterized by scanning electron microscopy (SEM) and X-ray photoelectron spectroscopy (XPS). The thermal decomposition properties were analyzed by thermogravimetric analysis (TGA), differential scanning calorimetry (DSC), and thermal-infrared spectrometry (DSC-FTIR) online. The results showed that the as-prepared material was a type of a novel superfine composite with the superfine RDX particles coated on the surface of Al flakes. XPS analysis indicated that a new Al–N bond was formed in the superfine RDX/Al composite and both physical and chemical absorptions existed between RDX and Al at the same time. The thermal decomposition temperature of RDX in the superfine RDX/Al composite had a shift of about 50 °C towards the lower temperature range compared with that of the neat superfine RDX when tested at four heating rates of 5, 15, 25 and 35 °C min^{-1}. Its activation energy value also decreased to 70.8 kJ mol^{-1} compared with that of the neat superfine RDX (119.6 kJ mol^{-1}). Moreover, thermal sensitivity of the superfine RDX/Al composite increased. DSC-FTIR analysis showed that the main decomposition products of the superfine RDX/Al composite were N_2O and CO_2 with nearly no NO and NO_2 detected. The formation of Al–N bond and reactive Al atoms are the main reasons for the notably advanced decomposition of RDX in the superfine RDX/Al composite.

Received 17th September 2018
Accepted 23rd October 2018

DOI: 10.1039/c8ra07650b

rsc.li/rsc-advances

1. Introduction

1,3,5-Trimethylene trinitramine (RDX) is the main energetic ingredient in both explosives and propellants. Its thermal decomposition characteristics directly affect the properties of explosives and propellants.[1–4] Thus, so far numerous papers have been published on the catalytic decomposition of RDX and many achievements have been made.[5–9]

Aluminum (Al), a type of fuel additive, is widely applied in explosive systems to improve the heat of explosion and power capability owing to its high calorific value and energy density.[10–13] It also plays an important role in propellants in seeking higher combustion efficiency and lower pressure exponent for the main fuel.[14–16]

Since RDX and Al usually exist simultaneously in many explosive and propellant formulations as main components, a large amount of research has been performed to study the performance, thermal behavior and decomposition mechanism of explosives and propellants containing Al and RDX.[17–23] Zhu *et al.*[19] studied the influence of different aluminum particle size on the thermal decomposition of RDX and found that Al with particle size of 40 nm catalyzed the decomposition of RDX. Fang *et al.*[20] prepared different propellants with graded aluminum powders containing superfine aluminum (SAl), and the experimental results indicated that SAl could effectively improve the combustion characteristics of propellants. Ye *et al.*[22] adopted generalized gradient approximation of the density functional theory (DFT) to study the adsorption and decomposition mechanism of RDX on the surface of Al and found that the attractive forces between Al atoms and RDX molecules induced breaking of the N–O and N–N bonds, leading to the decomposition of explosives on the surface of Al. However, the RDX/Al composites used in most of the studies were usually prepared by a simple physical mixing method, in which the reactive Al atoms were always covered by an Al_2O_3 layer that would decrease the contact between Al and RDX. Therefore, the analyses of the effect of Al on the decomposition properties of RDX will not be quite accurate.

In this study, a type of superfine RDX/Al composite energetic material (u-RDX/Al composite) was prepared by a mechanical

[a]National Special Superfine Powder Engineering Research Center of China, School of Chemical Engineering, Nanjing University of Science and Technology, Nanjing 210094, China. E-mail: superfine_jw@126.com; Fax: +86 25 84315042; Tel: +86 25 84315042

[b]Xi'an Modern Chemistry Research Institute, Xi'an 710065, China

ball-milling method. In order to explore the catalytic effect of Al on the decomposition of RDX in the as-prepared u-RDX/Al composite, a series of tests were performed. The morphology and structure of the u-RDX/Al composite were analyzed by SEM and XPS. The thermal characteristics of the u-RDX/Al composite were explored by TG and DSC analyses, while the decomposition mechanism was further studied using a DSC-FTIR coupling method. Furthermore, physical mixtures of superfine RDX and 15 μm Al (u-RDX/m-Al mixture) and mixture of superfine RDX and superfine Al (u-RDX/u-Al mixture) were prepared and characterized for comparison with the u-RDX/Al composite.

2. Experimental

2.1 Materials

The materials used in this study were 1 μm RDX (u-RDX), which was prepared in our laboratory from raw RDX (Gansu Yinguang Chemical Co., Ltd., China),[24] and 15 μm aluminum powders (m-Al) (Shanxi North Xing'an Chemical Industry Co., Ltd., China). The mass ratio of u-RDX and Al was constant, *i.e.*, 70/30, as used in many reported studies.[12,13,22]

2.2 Preparation of u-RDX/m-Al mixture

To improve the dispersity and uniformity of the u-RDX/m-Al mixture, a wet mixing technique was applied. First, 14 g u-RDX was added into a container with a small amount of ether and stirred for 30 min under ultrasonication. Second, 6 g m-Al was gradually added into the container. After stirring for another 30 min, the container was transferred to a vacuum drying oven and dried at 50 °C for 2 h. Finally, the dried sample was ground in a polished carnelian mortar for 15 min and then, the u-RDX/m-Al mixture was prepared.

2.3 Preparation of u-RDX/Al composite energetic material

In order to obtain a new type of composite material rather than a simple mixture of u-RDX and Al, the mechanical ball-milling technique, which could provide a powerful force to refine m-Al and generate the u-RDX/Al composite, was applied. First, 2 kg of 0.3 mm ZrO_2 was added as the milling medium in the cavity of a vertical ball mill. Then, 6 g m-Al powder was added together with 350 mL of ethyl acetate. Milling rate was set at 1100 rpm and maintained for 30 min. Second, 14 g of u-RDX particles were added into the mill. The milling rate was raised to 1300 rpm and maintained for about 10 h. Finally, the slurry and the milling media were poured out of the cavity and then filtrated to separate the u-RDX/Al composite slurry. The product was dried by vacuum freeze drying technology, as a result of which the u-RDX/Al composite sample was obtained.

2.4 Preparation of u-RDX/u-Al mixture

The mixture of u-RDX and superfine Al (u-Al) was also prepared to make a comparison with the u-RDX/m-Al mixture and the u-RDX/Al composite. u-Al was fabricated through a method similar to that mentioned in section 2.3. First, 2 kg of 0.3 mm ZrO_2, 10 g m-Al powders and 350 mL of ethyl acetate were added in the cavity of a vertical ball mill. The milling rate was set at 1100 rpm and maintained for about 5 h. Following this, the slurry and milling media were poured out of the cavity and then filtrated to separate the u-Al slurry. The u-Al content in the as-prepared slurry was then tested by solvent-evaporation method and the corresponding weight of u-RDX was confirmed based on the mass ratio of u-RDX and Al (70/30). Then, the u-RDX powder was added to the u-Al slurry and the mixture system was stirred at 500 rpm for 2 h. Finally, the u-RDX/u-Al mixture was dried by vacuum freeze drying technology.

2.5 Equipment and conditions

The size and morphology of the samples were characterized by a field emission scanning electron microscope (FE-SEM, Hitachi S-4800 II, Japan) operating between 2-10 kV.

The structures of samples were characterized by an ESCALAB 250Xi X-ray photoelectron spectrometer (XPS, Thermo Fisher Scientific, UK) with a monochromatic Al Kα radiation source (energy 1486.68 eV) at 164 W (10.8 mA and 15.2 kV) and a spot size of approximately 0.5 mm in diameter. During the analysis, vacuum was maintained $<2 \times 10^{-9}$ mbar. The electron energy analyser was operated with a pass energy of 20 eV, enabling high resolution of the obtained spectra. A step size of 0.05 eV was employed and each peak was scanned twice.

Thermogravimetric analysis (TG) and differential scanning calorimetric (DSC) experiments were performed using a SDT Q600 thermal analyzer (TA Instruments Co., Ltd., America). The weight of each of the samples was about 1 mg and the samples were placed in an alumina crucible. All the tests were performed under different heating rates of 5, 15, 25 and 35 °C min^{-1} from 50 to 400 °C with high-purity nitrogen flowing at a rate of 50 mL min^{-1}.

The DSC-FTIR tests for the u-RDX/Al composite, u-RDX/m-Al mixture and u-RDX/u-Al mixture were performed on a Netzsch STA449C (Germany) and Nicolet 5700 FTIR (America) coupling system. The sample (1.0 mg) was placed in an open aluminum crucible with heated at a rate of 20 °C min^{-1}. High-purity argon with a flow rate of 50 mL min^{-1} was used. The temperature of the gas cell and the gas tube between the DSC and FTIR was maintained at 200 °C.

3. Results and discussion

The morphology and particle sizes of m-Al, the u-RDX/m-Al mixture, the u-RDX/u-Al mixture and the u-RDX/Al composite were characterized by SEM, and the results are shown in Fig. 1.

As can be seen clearly from Fig. 1a, the size of raw micro aluminum particles was in the range from 5 μm to 20 μm, and their shapes were spherical-like with the surface covered by a rough Al_2O_3 layer. Fig. 1b shows that the surface of m-Al is coated by superfine RDX particles, but there are still many superfine RDX particles scattered around the mixture. Fig. 1c represents the SEM picture of the as-prepared u-RDX/u-Al mixture, which shows that the raw micro Al particles transformed into flake-like Al because of the good ductility of metallic Al, and the surface of the Al flakes was covered with u-

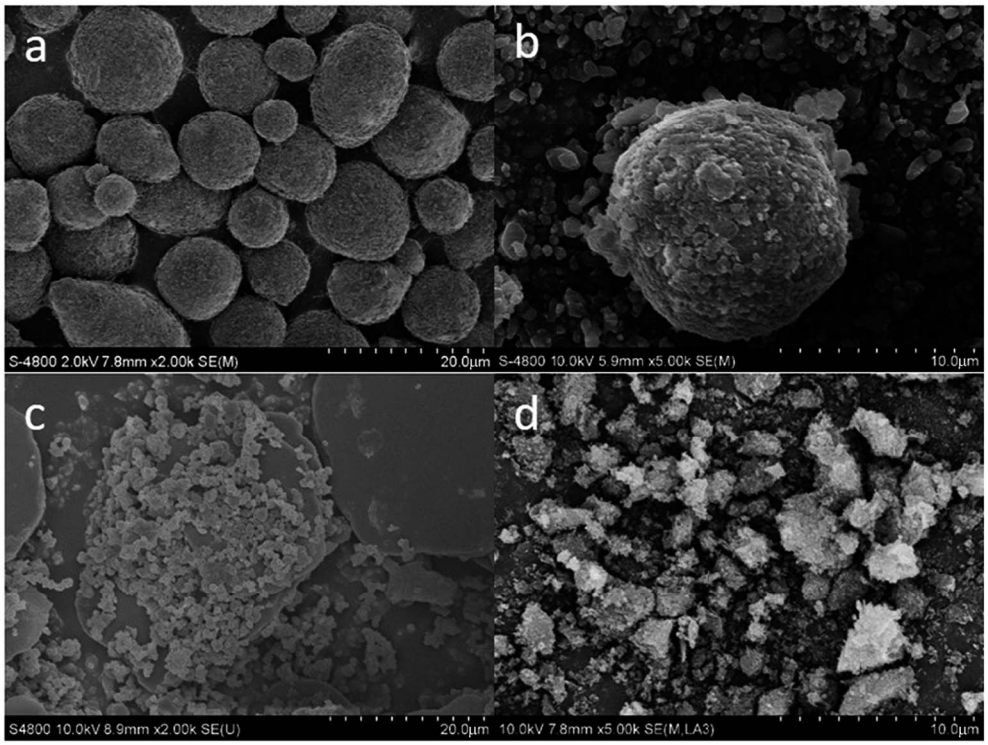

Fig. 1 SEM images of (a) m-Al, (b) u-RDX/m-Al mixture, (c) u-RDX/u-Al mixture and (d) u-RDX/Al composite.

RDX particles. The reactive Al was exposed and had good contact with u-RDX. As we can see from Fig. 1d, the u-RDX/Al composite has a different structure and shape superfine RDX and Al particles coexist in the milling system. The size of the flake-like Al particles decreased further due to the role of superfine RDX particles that act as a type of milling aid in the milling system. Furthermore, the granularity of the 1 μm RDX particles also decreased to a submicron scale. In fact, the superfine RDX particles were continuously embedded on the surface of Al flakes, thus forming an irregular layered structure under the powerful impact, friction, and shear forces provided by the mechanical ball-milling method. Hence, this method ensures that the Al atoms could have full contact with the RDX molecules in contrast to the u-RDX/m-Al mixture and u-RDX/u-Al mixture.

The structures of u-RDX/m-Al mixture, u-RDX/u-Al mixture and u-RDX/Al composite were analysed by XPS; the resulting Al 2p and N 1s XPS spectra of the three samples are presented in Fig. 2. In addition, the corresponding XPS peak values at different peak positions are listed in Table 1.

As shown in Fig. 2a, Al has two XPS peaks in the spectrum of the u-RDX/m-Al mixture. The peak at 74.1 eV corresponds to the Al–O bond of Al_2O_3, which was produced by the oxidation of pure Al. The peak at 71.8 eV corresponds to the Al–Al bond of pure Al in micro aluminum. Similarly, the N 1s spectrum also has two peaks at 407.1 eV and 401.4 eV, corresponding to N of $-NO_2$ and C–N–C in the superfine RDX. These results indicated that there was no chemical bond between superfine RDX and micro Al particles in the as-prepared u-RDX/m-Al mixture. The same curves could be observed in Fig. 2c and d revealing that the newly prepared u-Al also did not chemically adsorb the u-RDX despite the reactive Al atoms having full physical contact with RDX molecules.

However, there were apparent distinctions between the XPS spectra of u-RDX/Al composite (Fig. 2e and f) and that of either u-RDX/m-Al mixture (Fig. 2a and b) or u-RDX/u-Al mixture (Fig. 2c and d). It can be clearly observed that the Al 2p and N 1s peaks of the u-RDX/Al composite are divided into three peaks. The extra peak at 73.5 eV in the Al 2p spectrum could be ascribed to the Al–N bond (Fig. 2e), and the peak at 399.6 eV in the N 1s spectrum is assigned to N–Al bond (Fig. 2f). These results indicate that the Al–N bond exists in the u-RDX/Al composite and formed by the combination of N in RDX and Al under the strong mechanical milling force. Thus, it can be concluded that there exist physical absorption and chemical absorption simultaneously in the as-prepared u-RDX/Al composite; this result was consistent with the findings reported by Ye *et al.* in ref. 22.

The analyses of thermodynamics parameters would be beneficial for the better understanding of the thermolysis properties of the energetic materials. In this study, the thermal properties of neat u-RDX, u-RDX/m-Al mixture, u-RDX/u-Al mixture and u-RDX/Al composite were analyzed by TG-DSC measurements. The TG curves of neat u-RDX, u-RDX/m-Al mixture, u-RDX/u-Al mixture and u-RDX/Al composite at a heating rate of 35 °C min^{-1} are shown in Fig. 3, and the DSC traces of these samples at the heating rate of 5, 15, 25 and 35 °C min^{-1} are shown in Fig. 4.

It can be observed from Fig. 3 that the TG curve of the u-RDX/m-Al mixture is similar to that of neat u-RDX, and they suffered

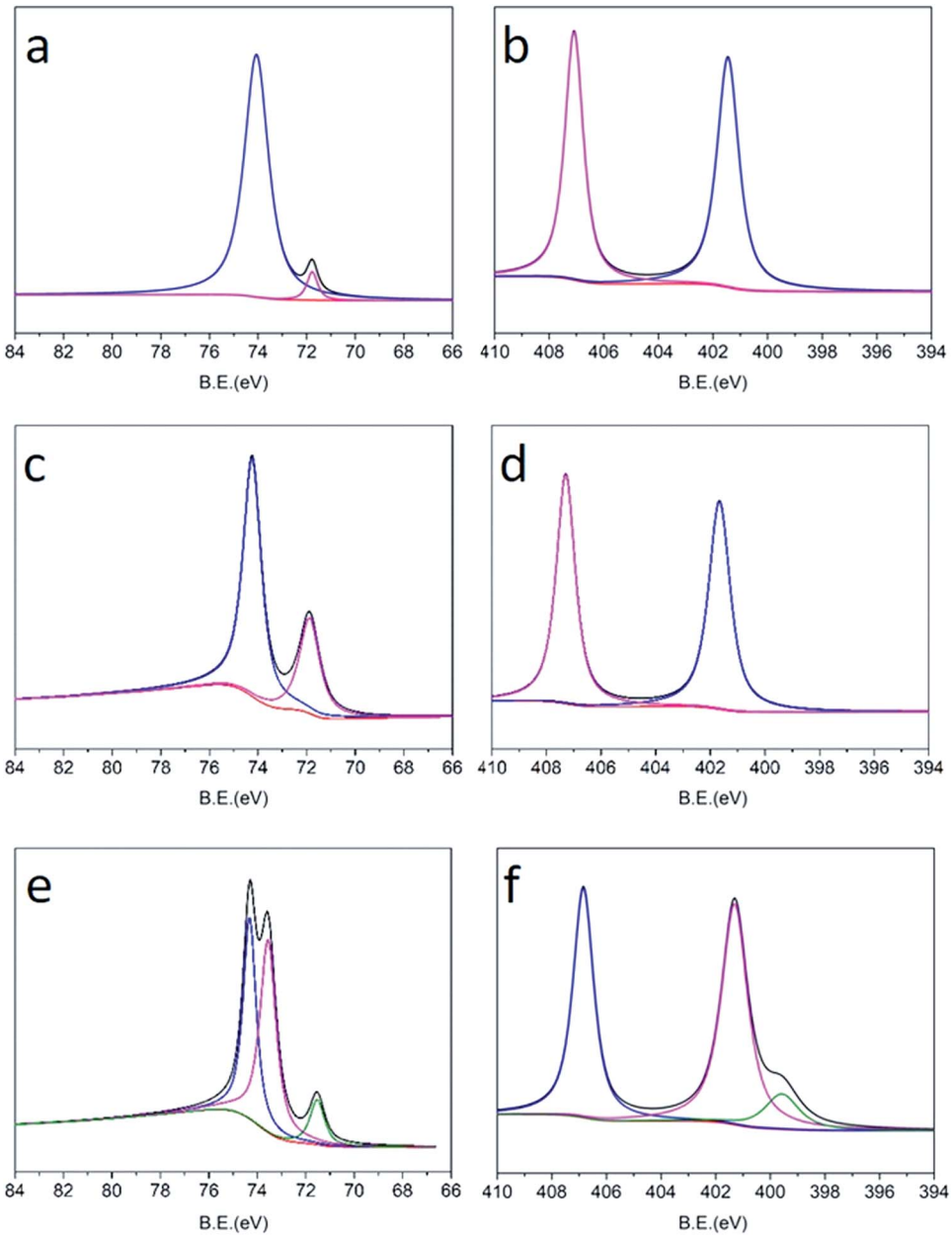

Fig. 2 XPS spectra of (a) Al 2p and (b) N 1s of the u-RDX/m-Al mixture, (c) Al 2p and (d) N 1s of the u-RDX/u-Al mixture, and (e) Al 2p and (f) N 1s of the u-RDX/Al composite.

Table 1 XPS peak values of Al 2p and N 1s of u-RDX/m-Al mixture, u-RDX/u-Al mixture and u-RDX/Al composite

	Al 2p (eV)			N 1s (eV)		
Samples	Al–O	Al–N	Al–Al	$-NO_2$	C–N–C	N–Al
u-RDX/m-Al mixture	74.1	—	71.8	407.1	401.4	—
u-RDX/u-Al mixture	74.2	—	71.9	407.3	401.7	—
u-RDX/Al composite	74.3	73.5	71.5	406.8	401.3	399.6

a large mass loss from 225 to 270 °C, indicating that m-Al had negligible effect on the decomposition of RDX. However, the TG curves of u-RDX/u-Al mixture and u-RDX/Al composite exhibit different traces. It is apparent that the onset and final temperatures of weight loss in the u-RDX/u-Al mixture and u-RDX/Al composite were lowered. As the temperature increased, the u-RDX/u-Al mixture exhibited a mass loss process from 210 to 250 °C, while the mass of u-RDX/Al composite reduced in the range of 150 to 220 °C. Moreover, due to the release of absorbed gases or moisture from the surface of the u-RDX/Al composite, the mass of u-RDX/Al composite decreased slowly at the initial stage of weight loss.[25,26] After the completion of the reaction, the mass percentages of the u-RDX/u-Al mixture and the u-RDX/Al composite were about 35% and 40% at 350 °C, respectively, which were 30% higher than the corresponding mass percentage of Al in the u-RDX/m-Al mixture. This difference was mainly attributed to the reaction of the gas products evolving

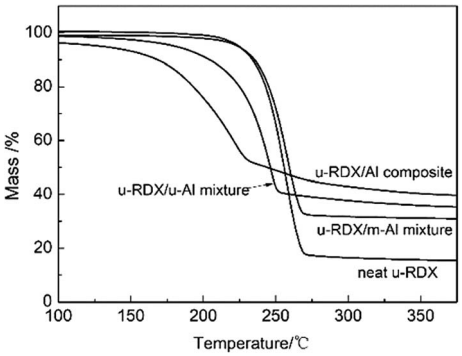

Fig. 3 TG curves of neat u-RDX, u-RDX/m-Al mixture, u-RDX/u-Al mixture and u-RDX/Al composite at the heating rate of 35 °C min^{-1}.

from the decomposition process of u-RDX with the reactive Al atoms in u-Al.

Fig. 4a and b show the similar curves comprising a melting endotherm followed by exothermic decomposition for neat u-RDX and u-RDX/m-Al mixture. It can be found that the exothermic peak temperature (T_P) of the u-RDX/m-Al mixture shifted by about 1–3 °C towards lower temperature compared with the peak temperatures of neat u-RDX, which could be ascribed to the thermal conductivity of m-Al. The DSC curve of the u-RDX/u-Al mixture exhibited the same traces as that of u-RDX and the u-RDX/m-Al mixture. However, the T_P of u-RDX in the u-RDX/u-Al mixture had a larger shift of approximately 15 °C towards the lower temperatures compared with that of neat u-RDX, which was consistent with the TG results. However, there was only an exothermic peak for the u-RDX/Al composite and the melting endotherm did not exist, as evident from Fig. 4d. The melting process was covered within the exothermic process because of the advancement of reaction onset temperature, which was lower than the melting temperature of RDX. The T_P of RDX in the u-RDX/Al composite was much lower than that of neat u-RDX at all the four heating rates with a difference of about 50 °C.

The kinetic parameters for RDX decomposition were calculated according to the exothermic peak temperature dependence as a function of heating rate (Kissinger correlation).[27] The exothermic peak temperatures at 5, 15, 25 and 35 °C min^{-1} and the calculated activation energy values (E_a) of neat u-RDX, u-RDX/m-Al mixture, u-RDX/u-Al mixture and u-RDX/Al composite under different milling times of 3 h, 6 h and 10 h are tabulated in Table 2.

$$\ln\left(\frac{\beta}{T_P^2}\right) = -\frac{E_a}{RT_P} + \ln\left(\frac{AR}{E_a}\right) \quad (1)$$

where β is the heating rate in degrees celsius per minute, T_P is the maximum exothermic peak temperature, R is the ideal gas

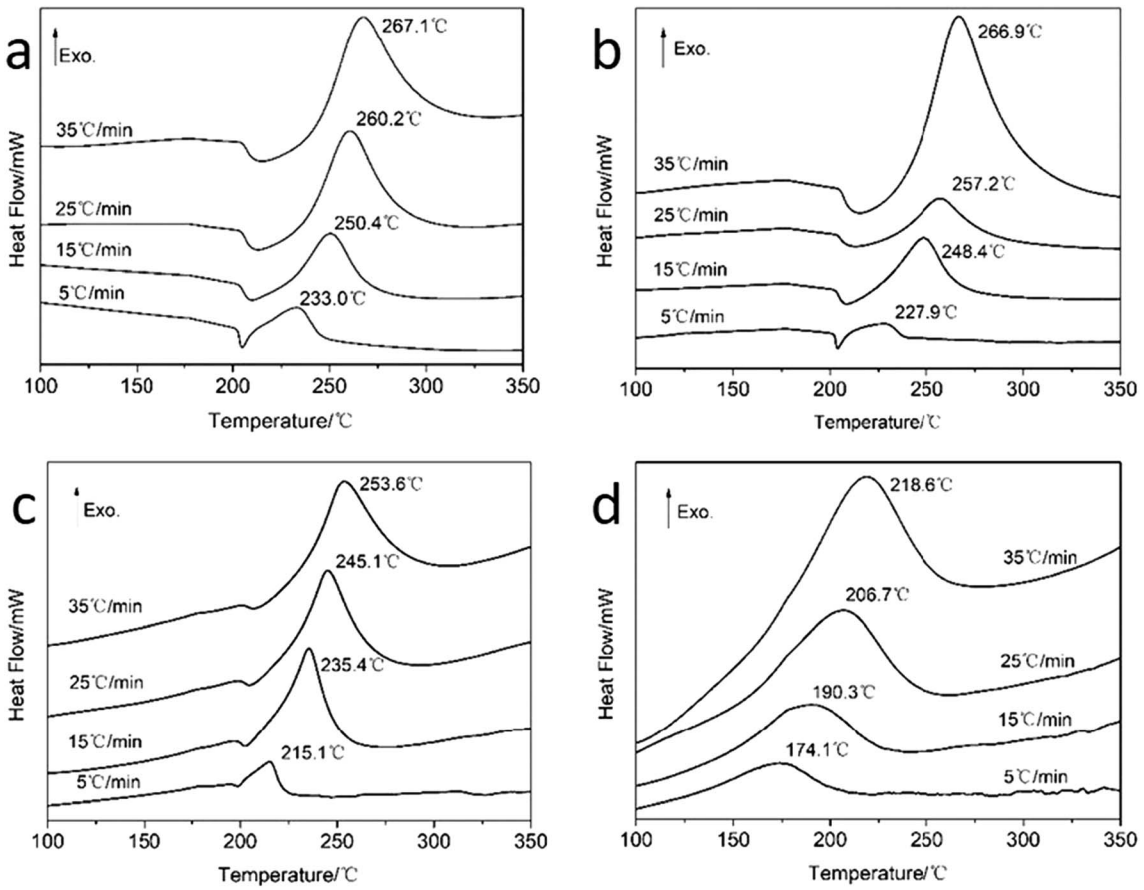

Fig. 4 DSC curves of (a) neat u-RDX, (b) u-RDX/m-Al mixture, (c) u-RDX/u-Al mixture and (d) u-RDX/Al composite at heating rates of 5, 15, 25 and 35 °C min^{-1}.

Table 2 DSC peak temperatures and kinetic parameters for neat u-RDX, u-RDX/m-Al mixture, u-RDX/u-Al mixture and u-RDX/Al composite under milling times of 3 h, 6 h and 10 h at 5, 15, 25 and 35 °C min^{-1}

Samples	$T_{P,\beta}$ (°C)				E_a (kJ mol^{-1})	A (min^{-1})	R^2
	$T_{P,5}$	$T_{P,15}$	$T_{P,25}$	$T_{P,35}$			
Neat u-RDX	233.0	250.4	260.2	267.1	119.6	6.36×10^{11}	0.9975
u-RDX/m-Al mixture	227.9	248.4	257.2	266.9	105.7	4.60×10^{8}	0.9951
u-RDX/u-Al mixture	215.1	235.4	245.4	253.6	100.8	2.62×10^{8}	0.9984
u-RDX/Al composite-3 h	201.3	218.1	230.8	235.4	103.1	1.09×10^{9}	0.9905
u-RDX/Al composite-6 h	181.6	197.9	212.0	220.8	83.8	1.90×10^{7}	0.9766
u-RDX/Al composite-10 h	174.1	190.3	206.7	218.6	70.8	7.74×10^{5}	0.9542

constant, E_a is the activation energy, and A is the pre-exponential factor.

It can be clearly observed that the E_a value of u-RDX in the u-RDX/Al composite decreased to only 70.8 kJ mol^{-1} compared with 119.6 kJ mol^{-1} of neat u-RDX, 105.7 kJ mol^{-1} of the u-RDX/m-Al mixture, and 100.8 kJ mol^{-1} of the u-RDX/u-Al mixture. These results showed that u-RDX in the as-prepared composite easily decomposed with the increase in temperature.

As can be seen from Table 2, T_P and E_a values of the u-RDX/Al composite decreased with the increase in milling time. The decomposition temperature of u-RDX in the u-RDX/Al composite with 3 h of milling time had a significant reduction by 30 °C compared with that of the neat u-RDX. This difference in temperature increased to 50 °C when the milling time was extended to 10 h. In other words, the contact between u-RDX molecules and Al atoms became highly sufficient in the milling system with the increase in milling time, which led to the formation of more Al–N bonds. This may be a possible reason for the easy catalytic decomposition of u-RDX in the u-RDX/Al composite.

The critical ignition temperature of thermal explosion (T_b) should be the lowest to ensure safety of an explosive when it is heated without any thermal dissipation.[28] In this study, the critical temperatures for neat u-RDX, u-RDX/m-Al mixture, u-RDX/u-Al mixture and u-RDX/Al composite were calculated using eqn (2) and (3),[29] and the results are shown in Table 3.

$$T_i = T_0 + b\beta_i + c\beta_i^2 + d\beta_i^3 \ (i = 1, 2, 3, 4) \quad (2)$$

where T_0 is T_P at $\beta \rightarrow 0$, b, c and d are coefficients, β_i is the heating rate (K min^{-1}), and T_i is the peak temperature at β_i.

$$T_b = \frac{E_a - \sqrt{E_a^2 - 4E_aRT_0}}{2R} \quad (3)$$

Table 3 Critical temperature of thermal explosion for neat u-RDX, u-RDX/m-Al mixture, u-RDX/u-Al mixture and u-RDX/Al composite under different milling time of 3 h, 6 h and 10 h

Samples	T_0 (°C)	T_b (°C)
Neat u-RDX	219.9	223.4
u-RDX/m-Al mixture	209.3	212.8
u-RDX/u-Al mixture	198.0	201.3
u-RDX/Al composite-3 h	192.7	195.8
u-RDX/Al composite-6 h	173.7	176.8
u-RDX/Al composite-10 h	167.5	171.0

where E_a is activation energy (J mol^{-1}) and R is the gas constant (8.314 J k^{-1} mol^{-1}).

Table 3 shows that the critical temperatures of neat u-RDX, u-RDX/m-Al mixture and u-RDX/u-Al mixture are 223.4 °C, 212.8 °C and 201.3 °C, respectively, while the T_b values of the u-RDX/Al composite prepared under milling times of 3 h, 6 h and 10 h were much lower (about 195.8 °C, 176.8 °C and 171.0 °C, respectively). These results indicated that the thermal sensitivity of u-RDX increased with the addition of Al and the increase in degree of sensitivity was even greater on adopting mechanical ball-milling method and extending the milling time compared with that of physical blending.

DSC-FTIR analyses were conducted to research the decomposition mechanisms of u-RDX/m-Al mixture, u-RDX/u-Al mixture and u-RDX/Al composite. The FTIR results are shown in Fig. 5. The total absorbance of gaseous products in u-RDX/m-Al mixture, u-RDX/u-Al mixture and u-RDX/Al composite are presented in Fig. 5a, c and e, respectively. Five different points were chosen from the curves in Fig. 5a, c and e, and the corresponding FTIR spectra of the gas products are shown in Fig. 5b, d and f.

According to these spectra, the main gas products for the u-RDX/m-Al mixture were N_2O, CO_2 and NO_2 besides a few NO and H_2O molecules. Fig. 5d shows that the main gas products evolved from the u-RDX/u-Al mixture are N_2O and CO_2. The amount of NO and NO_2 molecules decreased compared with that from the u-RDX/m-Al mixture. While it can be seen from the spectra in Fig. 5f that the main gas products for u-RDX/Al composite are N_2O and CO_2, the amount of NO and NO_2 molecules was too low to be detected. It is easy to conclude that N_2O and CO_2 are the main decomposition products evolved from u-RDX/m-Al mixture, u-RDX/u-Al mixture, or u-RDX/Al composite. With the increase in temperature, the decomposition of RDX initiated by the bond cleavage of N–NO_2, which was the weakest bond, due to which the $\cdot NO_2$ radical formed. Then, $\cdot NO_2$ would react with –C– and –N– to form N_2O and CO_2. Moreover, N_2O would be formed rather than CO_2 due to the higher electronegativity of –N– than that of –C–.[30–32] Therefore, the signal of N_2O is much stronger in the FTIR spectra of u-RDX/m-Al mixture and u-RDX/u-Al mixture. Furthermore, it can be observed that the ratio of CO_2 to N_2O in the u-RDX/Al composite is larger than that in the u-RDX/m-Al mixture and the u-RDX/u-Al mixture, which is mainly due to the formation of the Al–N bond that consumes –N–.

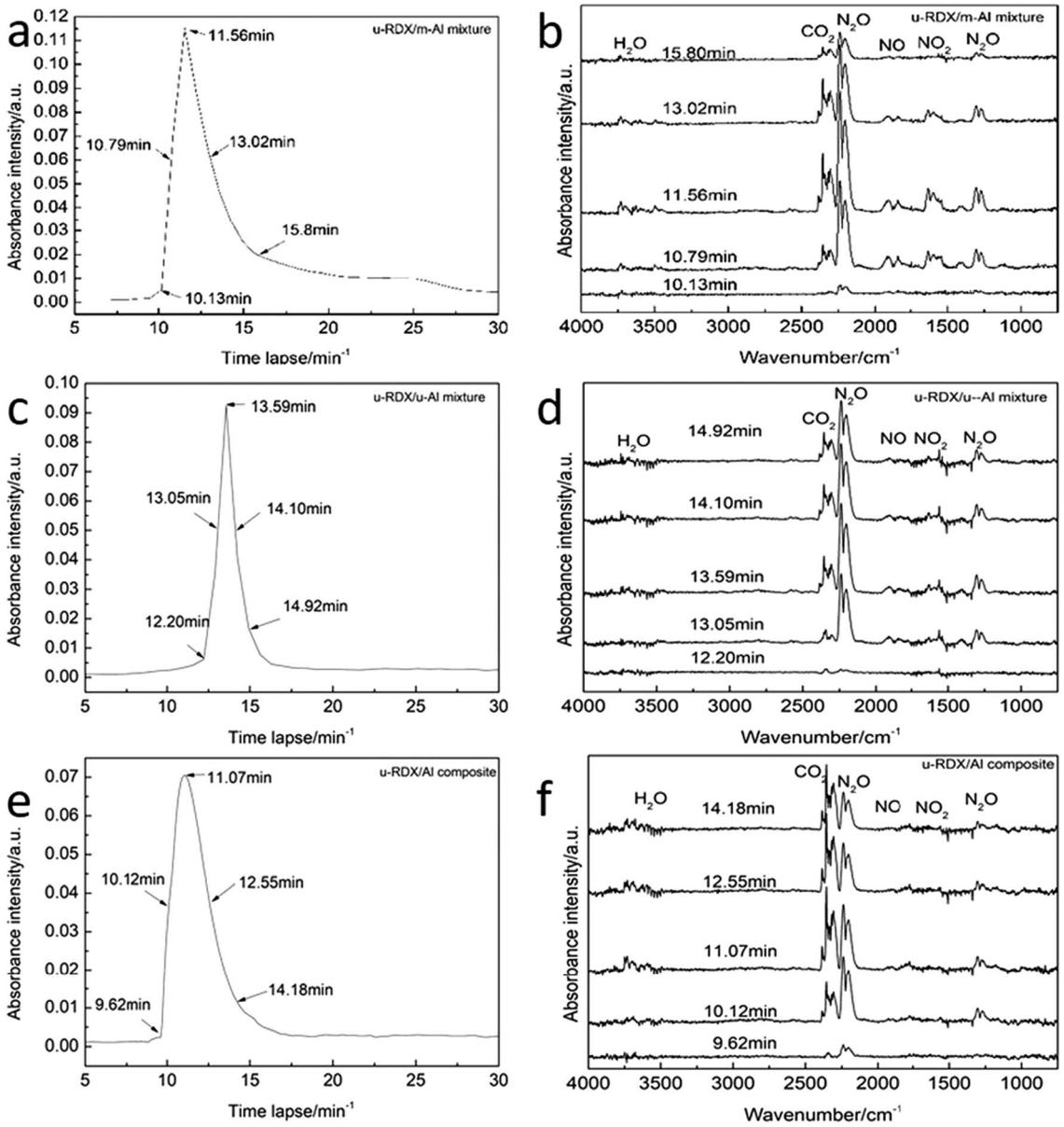

Fig. 5 FTIR spectra of u-RDX/m-Al mixture, u-RDX/u-Al mixture, and u-RDX/Al composite: (a, c and e) total absorbance of gas products; (b, d and f) FTIR spectra of gas products intercepted at different times.

The dependence of absorbance intensity of N_2O and NO_2 from the u-RDX/m-Al mixture, u-RDX/u-Al mixture and u-RDX/Al composite on temperature is further depicted in Fig. 6 and 7. There was no significant difference between the onset and peak temperatures corresponding to the detected absorbance intensity of N_2O and NO_2 evolved from the u-RDX/m-Al mixture based on the IR spectra in Fig. 6a and 7a. However, it can be clearly seen that the onset and peak temperatures corresponding to the intensity of N_2O from the u-RDX/Al composite (Fig. 6b) and u-RDX/u-Al mixture (Fig. 6c) are distinctly lower than that of u-RDX/m-Al mixture, indicating that the decomposition of RDX in u-RDX/u-Al mixture and u-RDX/Al composite occurs earlier, corresponding to the findings from TG and DSC analyses. Moreover, the intensity of NO_2 from u-RDX/Al composite (Fig. 7b) and u-RDX/u-Al mixture (Fig. 7c) was nearly zero during the decomposition of u-RDX, which indicated that the O atoms in RDX were possibly caught by some reducing agents that existed in u-RDX/u-Al mixture and u-RDX/Al composite rather than the u-RDX/m-Al mixture.

When we compared the u-RDX/m-Al mixture and u-RDX/u-Al mixture, we found that the main difference between the two mixtures was the shape of the Al particles. The Al particles in the u-RDX/u-Al mixture were in the form of flakes that had bigger specific surface area and more reactive Al atoms on the surface and could have full contact with u-RDX. This difference caused the advanced decomposition of u-RDX in the u-RDX/u-Al mixture and hence, fewer NO_2 molecules formed. Thus, it can be concluded that the as-prepared flake-like Al particles have a catalytic effect on the decomposition of RDX due to its better thermal conductivity and reaction with the decomposition

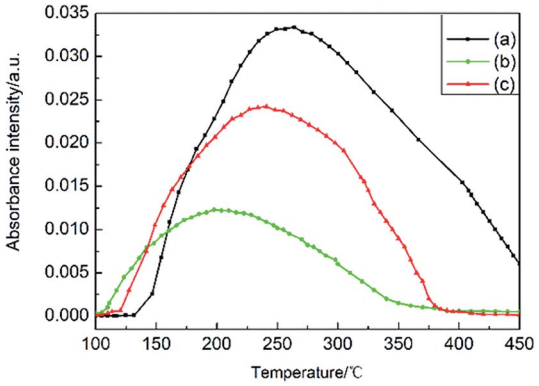

Fig. 6 Temperature dependency of FTIR intensity of N_2O from (a) u-RDX/m-Al mixture, (b) u-RDX/Al composite, and (c) u-RDX/u-Al mixture.

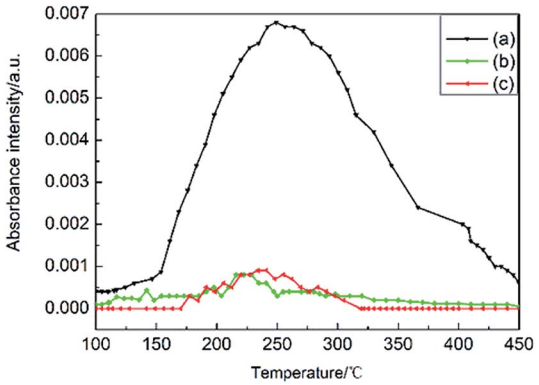

Fig. 7 Dependence of FTIR intensity of NO_2 from (a) u-RDX/m-Al mixture, (b) u-RDX/Al composite, and (c) u-RDX/u-Al mixture on temperature.

products during the decomposition of RDX compared with normal m-Al particles.

The main difference between the u-RDX/u-Al mixture and the u-RDX/Al composite is that a new Al–N bond was formed in the u-RDX/Al composite due to the mechanical ball milling method. This resulted in the decomposition of u-RDX in the u-RDX/Al composite at a greatly advanced temperature range. Thus, it can be concluded that the Al–N bond plays an important role in the decomposition of u-RDX. Moreover, it can be inferred that the Al–N bond may dominate the decomposition of u-RDX than the flake-like Al particles based on the findings from DSC analyses. Furthermore, it is evident that the catalytic decomposition of RDX in the u-RDX/Al composite improved with the increase in milling time because of the formation of more Al–N bonds, more reactive Al, and improvement in the thermal conductivity of Al.

Overall, the decomposition mechanisms of RDX in the u-RDX/Al composite prepared by mechanical ball milling method are likely dependent on the formation of Al–N bonds and reactive Al. The strong Al–N bond led to weakening of the N–N bond and N–O bond, which split more easily and promoted the decomposition of u-RDX.[17] Furthermore, more reactive Al atoms in the Al particles exposed during the milling process. The redox reaction between the fuel (reactive Al atoms) and the oxidizer (the decomposition products) would proceed, which accelerated the decomposition of u-RDX. Furthermore, the thermal conductivity was likely non-negligible. The smaller the particle size, the better the thermal conductivity. During the milling process, the size of the Al particles was decreased and hence, the thermal conductivity increased, leading to faster endothermic process with the increase in temperature so that the u-RDX particles would decompose much ahead of the other materials tested in this study.

4. Conclusions

(1) A superfine RDX/Al composite energetic material was successfully prepared by the mechanical ball-milling method, in which both physical absorption and chemical absorption exist between u-RDX and Al.

(2) From the u-RDX/m-Al mixture, the main decomposition products were N_2O, CO_2 and NO_2, while from the u-RDX/u-Al mixture and u-RDX/Al composite, the main products were N_2O and CO_2 with almost no NO_2.

(3) A series of analyses revealed that the advanced decomposition of u-RDX in the u-RDX/Al composite occurred due to the reactive Al and the Al–N bonds, which played a leading role. The degree of decrease in the decomposition temperature was more notable with the increase in milling time. This indicated that the exothermic decomposition properties of u-RDX could be controlled by the adjustment of Al content and the mechanical ball-milling process. This study will be beneficial for obtaining new formula designs and potential applications for the RDX/Al composite.

Conflicts of interest

There are no conflicts to declare.

Acknowledgements

This study was financially supported by National Natural Science Foundation of China (No. 51606102, No. 21805139), the Fundamental Research Funds for the Central Universities (No. 30918011312), Basic Product Innovation Technology Research Project of Explosives and Youth Scientific and Technological Innovation Project (QKCZ201713).

Notes and references

1 K. K. Kuo, G. A. Risha and B. J. Evans, *MRS Proc.*, 2003, 800.
2 W. H. Hsieh and W. Y. Li, *Propellants, Explos., Pyrotech.*, 2015, **23**, 128–136.
3 G. T. Sutherland, L. J. Brousard and J. F. Leahy, *J. Energ. Mater.*, 2004, **22**, 181–197.
4 D. M. Badujar, M. B. Talawar, S. N. Asthana and P. P. Mahulikar, *J. Hazard. Mater.*, 2008, **151**, 289–305.
5 Y. P. Tong, Y. P. Wang, Z. X. Yu, X. Wang, X. J. Yang and L. D. Lu, *Mater. Lett.*, 2008, **62**, 889–891.

6 T. X. Liu, B. X. Li, Y. G. Hao and Z. Y. Yao, *Chem. Eng. J.*, 2014, **244**, 382–390.
7 P. Ujwol, K. Henning, N. Rodrigo, A. Sahar, J. Vladislav, M. Philipp, A. Hasan, S. Alberto, S. Helmut and K. Dietmar, *Nano Energy*, 2014, **6**, 167–172.
8 T. Wei, Y. Zhang and K. Xu, *RSC Adv.*, 2015, **5**, 70323–70328.
9 Y. Zhang, T. Wei and K. Xu, *RSC Adv.*, 2015, **5**, 75630–75635.
10 M. A. Cook, A. S. Filler and R. T. Keyes, *J. Phys. Chem.*, 1957, **61**, 189–196.
11 H. Hui, H. H. Jian and H. Yong, *Explos. Shock Waves*, 2006, **26**, 7–11.
12 N. Muravyev, Y. Frolov and A. Pivkina, *Propellants, Explos., Pyrotech.*, 2010, **35**, 226–232.
13 P. Langen and P. Barth, *Propellants, Explos., Pyrotech.*, 1979, **4**, 129–131.
14 K. Jayaraman, K. V. Anand and D. S. Bhatt, *J. Propul. Power*, 2009, **25**, 471–481.
15 F. Tepper and G. V. Ivanov, *Int. J. Energ. Mater. Chem. Propuls.*, 1997, **4**, 636–645.
16 M. C. J. Van Ramshorst, G. L. D. Benedetto and W. Duvalois, *Propellants, Explos., Pyrotech.*, 2016, **41**, 700–708.
17 N. Umezawa, R. K. Kalia and A. Nakano, *J. Chem. Phys.*, 2007, **126**, 234702.
18 L. Liang, J. Y. Wang and J. Dong, *J. Explos. Propellants*, 2009, **32**, 75–78.
19 Y. L. Zhu, H. Huang and H. Ren, *J. Energ. Mater.*, 2013, **31**, 178–191.
20 C. Fang and S. Li, *Propellants, Explos., Pyrotech.*, 2002, **27**, 34–38.
21 C. Weir, M. L. Pantoya and M. A. Daniels, *Combust. Flame*, 2013, **160**, 2279–2281.
22 C. C. Ye, F. Q. Zhao and S. Y. Xu, *J. Mol. Model.*, 2013, **19**, 2451–2458.
23 Y. F. Zheng, H. Nan and P. Xi, *J. Explos. Mater.*, 2015, **5**, 13–17.
24 J. Liu, W. Jiang and F. S. Li, *Acta Armamentarii*, 2013, **34**, 174–180.
25 L. G. Guo, W. L. Song and M. L. Hu, *Appl. Surf. Sci.*, 2008, **254**, 2413–2417.
26 Z. H. Wang, C. J. Choi and B. K. Kim, *Carbon*, 2003, **41**, 1751–1758.
27 H. E. Kissinger, *Anal. Chem.*, 1957, **29**, 1702–1706.
28 Y. Luo, P. Chen and F. Q. Zhao, *Chin. J. Chem.*, 2010, **22**, 1219–1224.
29 T. Zhang, R. Hu and Y. Xie, *Thermochim. Acta*, 1994, **244**, 171–176.
30 C. J. Wu and L. E. Fried, *J. Phys. Chem. A*, 1997, **101**, 8675–8679.
31 Y. Wang, X. Song and D. Song, *J. Hazard. Mater.*, 2016, **312**, 73–83.
32 X. L. Song, Y. Wang and C. W. An, *AIP Adv.*, 2018, **8**, 065009.